Capturing Marangoni flow via synchrotron imaging of selective laser melting

IOP Conf. Series: Materials Science and Engineering **861** (2020) 012010 doi:10.1088/1757-899X/861/1/012010

Capturing Marangoni flow via synchrotron imaging of selective laser melting

S J Clark[1,2], C L A Leung[1,2], Y Chen[1,2], L Sinclair[1,2], S Marussi[1,2] and P D Lee[1,2]

[1] Mechanical Engineering, University College London, WC1E 7JE, UK
[2] Research Complex at Harwell, Harwell Campus, Didcot, OX11 0FA, UK

E-mail: samuel.clark@ucl.ac.uk

Abstract. Marangoni flow has a substantial influence on the quality of components fabricated via laser powder bed fusion (LPBF). However, Marangoni flow in melt pools is rarely quantified due to the opacity of liquid metals and the necessity for *in situ* evaluation. Here we report the findings of high-temporal-resolution synchrotron x-ray radiography experiments tracking the flow in the melt-pool. Dense, highly attenuating tungsten carbide particles are seeded within an elemental powder blend of aluminium and copper of varying composition. Due to the extremely high temporal resolution of greater than 50 kfps at the 31-ID-B beamline at the Advanced Photon Source, USA, we can track the position of tracer particles from frame to frame. This data provides valuable process guidance for optimising mixing and informs the development and validation of multiphysics models.

1. Introduction

Marangoni flow has a substantial influence on the quality of laser additive manufactured components. It has previously been shown that unstable melt flow can be responsible for increased porosity and surface imperfections in laser powder bed fusion (LPBF) [1]. The effects of melt-pool flow have been studied in related process such welding where the magnitude of the velocity and the direction of the flow has been shown to have a potent influence on the weld pool geometry [2–7]. The understanding of the melt-pool flow nature is thus critical for microstructural and process control. However, the nature of the Marangoni flow is rarely evaluated due to the opacity of liquid metals and the necessity for *in situ* evaluation.

Previous studies have deployed the use of highly attenuating tungsten tracers in x-ray experiments to track the melt-pool flow using high-speed synchrotron x-ray radiography [8] and using an innovative lab-source based stereographical apparatus [9] in arc welding and high power laser welding respectively. Leung *et al.* [10] traced the motion of gas porosities during the laser additive LPBF of invar powders during a build simulating an overhang condition where the deposit rests on powder rather than a base plate or previous layers of the build. Recently, Guo *et al.* [11] have reported the findings of their high-speed synchrotron radiographic studies of melt-pool flow tracking in AlSi10Mg and Al-6061. Guo *et al.* [11], revealed a sharp contrast between the full field flow patterns under both conduction-mode and keyhole-mode melting processing parameters. In conduction-mode, the melt pool was shown to exhibit a simple flow analogous to the glow platters typically observed in arc welding [8]. However, the flow pattern in depression-mode was observed to be complicated, and it was suggested that this was due to the coaction of driving forces. Marangoni flow dominates behind the laser whereas at and close to the laser-matter interaction site vaporization dominates the fluid flow along the keyhole walls

combined with pressure and buoyancy effects. It is suggested that in order for an *in situ* alloying to be viable means of synthesizing novel alloys in LPBF [12, 13]. For this to be feasible it is suggested that the Marangoni flow in the melt-pool must be sufficient in order that the alloying elements in the melt-pool be homogeneously blended. In this work, we explore the potential for *in situ* alloying strategies via visualising the Marangoni flow in the melt-pool. We report the findings of our synchrotron x-ray radiography flow tracking experiments performed independently and without knowledge of the experiments by Guo *et al.* [11]. The reported flow pattern in keyhole-mode is schematically shown in figure 1.

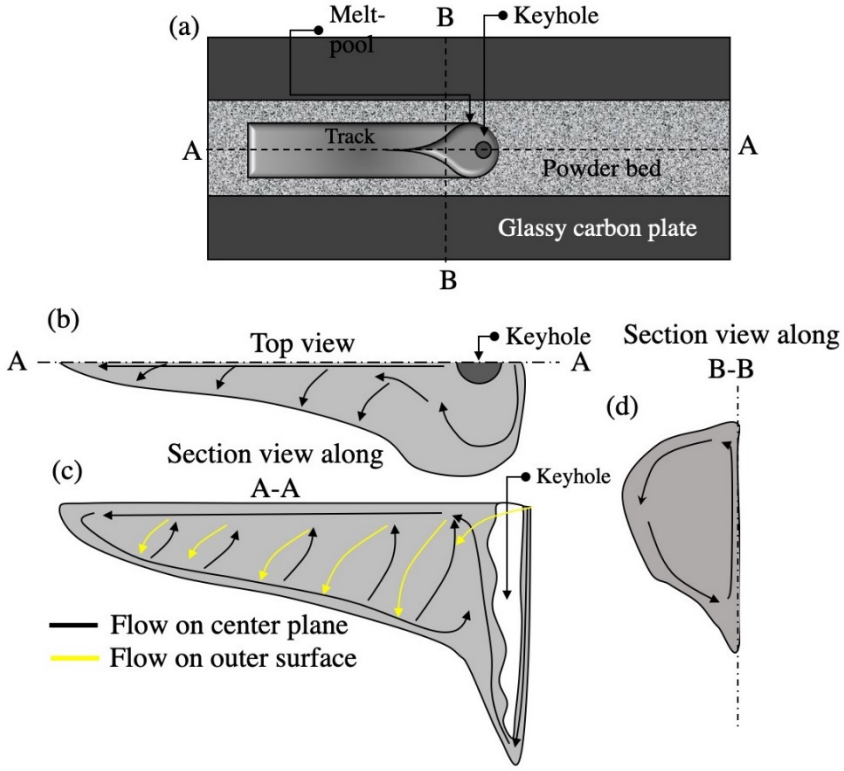

Figure 1. (a) Schematic top view of the melt-pool and track, (b) top view of the melt-pool annotated with the flow pattern, (c) section view along A-A annotating the flow observed on the central plane and that of the outer surface, (d) section view along B-B annotated with the in-plane flow pattern.

2. Materials and methods

The *in situ* and *operando* process replicator ISOPR is an evolution of the original design used in previous studies [10, 14, 15]. The apparatus consists of a miniaturised LPBF system with the functionality to automatically lower the substrate and spread a layer powder. The multi-layer capability facilitates the faithful replication of the fabrication of multilayer parts associated with industrial LPBF machines. The laser system consists of a continuous wave 520 W Yb-doped fibre laser, with a wavelength of 1070 ± 10 nm (IPG YLR-500-AC, USA). The laser optics consisted of a collimator followed by a beam expander, and finally, an X–Y galvanometer scanner (intelliSCAN$_{de}$ 30, SCANLAB GmbH, Germany) coupled with an f-theta lens. The optical system was tuned to produce a spot size of $\approx 42\ \mu m$, which was determined through measuring the averaged throat of the keyhole observed in the x-ray radiographs, at the powder bed surface.

The unique ISOPR environmental chamber is shown in figure 2. It contains a miniature powder bed which is formed from a substrate of 99% pure aluminium (Goodfellow, UK) with dimensions of 46 x 17 x 0.8 mm sandwiched between two glassy carbon plates of 1 mm in thickness (HTW, Germany). The

substrate is remotely lowered by ≈60 µm to create a cavity of 46 x 0.06 x 0.8 mm. A schematic view of the sample assembly is shown in figure 1(a). Gas atomised (GA) Al-6061 series powder (Goodfellow, UK) with a particle size range of 15 – 45 µm was blended by manually tipping the powders back and forth with 50 wt.% of tungsten powder (Alfa Aesar, USA) with a maximum particle size of 12 µm. The blended powders were deposited evenly within the cavity using a gravity-fed powder hopper subsystem. Prior to operation, the environmental chamber is evacuated and back-filled to a modest positive pressure of <10 kPa with technical grade argon gas at a flow rate of 4 L min^{-1}, this flow of argon was then maintained throughout the experiment.

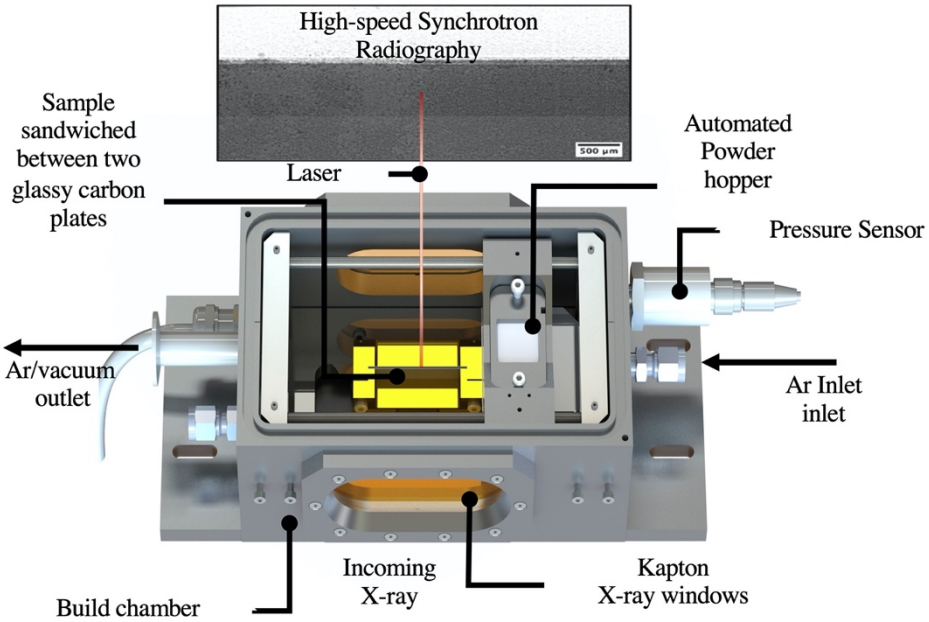

Figure 2. Schematic diagram of the ISOPR LPBF process replicator

In situ X-ray radiography experiments were undertaken at the 32-ID-B imaging beamline at the Advanced Photon Source (APS), in Chicago, USA. Recently, this beamline has been used for several high-speed radiographic studies of powder bed fusion [11, 16–18]. The beamline was configured to achieve a polychromatic pink beam with the harmonic energy at 24 keV and an energy bandwidth of 5-7%. The ISOPR process replicator is positioned directly in the path of the beam such that it is selectively attenuated by the sample assembly contained within. The attenuated x-ray beam is then converted to optically visible light using a 100 µm thick LuAg:Ce scintillator and recorded with a FASTCAM SA-Z (Photron, USA) with 10x magnification, at 50 kfps and a pixel size of 1.87 µm. The resultant field of view was 512 pixels (0.96 mm) in width by 680 pixels (1.27 mm) in height. In this experiment, the laser traverses the powder bed at a velocity of 756.7 mm s^{-1} (calibrated by tracking the position of the keyhole) over the powder bed with an output power of 500 W.

3. Results and discussion

3.1. Melt-pool reconstruction and quantification

To quantify the dimensions of the melt-pool, the stack of 1024 radiographs were processed via a local-temporal background subtraction implemented in Matlab (MathWorks inc., USA). Each image is background-subtracted through looping progressively through the stack dividing each image by its 50 nearest neighbours. A median image of the resultant sub-stack of 50 images is computed. The effect of

this process is to remove any features in each image which are on average common to 50 nearest neighbours. Due to the large size of the melt-pool and the limited field-of-view of the imaging setup in no single acquired raw image is the entire melt-pool visible. Figure 3 shows a reconstructed image of the melt-pool, it is generated by extracting the velocity of the laser beam (in this case 756.7 mm s^{-1}) by tracking the bottom of the keyhole and then translating each image such that the laser beam appears to be stationary. Computing a median image of the translated stack yields a single image containing the entire melt-pool. It is shown that with the processing parameters outlined above the melt pool is of 2100 µm measured from the rear wall of the keyhole to the final point to solidify furthermore, the keyhole is shown to be 492 µm in depth measured from the top surface of the 99% pure aluminium substrate plate. Ahead of the keyhole a thin film 28 µm thick is melted. The projected area of the melt-pool behind the keyhole is 0.38 mm^2.

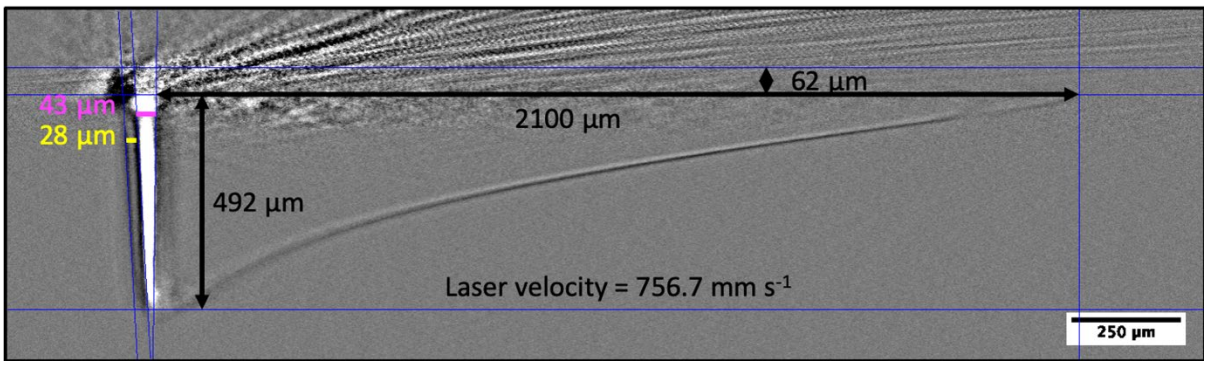

Figure 3. Reconstructed melt-pool

3.2. Elucidation of the flow pattern and projected tracer speed

Figure 4(a)-(e) shows a time series of high-magnification images of the region around the keyhole the passage of a single tungsten tracer particle has been highlighted in yellow. The average speed of highlighted particle was measured to be 968.8 mm s^{-1} in the moving reference frame of the laser. In our experiments, tungsten tracer particles were not observed to be transported via the thin melt ahead of the front keyhole wall. It is suggested that the experimentally observed high-velocity vapour jet emanating from keyhole [19–21] denudes any powder directly in the path of the laser beam via entrainment. It appears that powder particles typically bypass the keyhole joining the melt-pool from the outer surface. Figure 4(f) shows a composite image generated by extracting the pixelwise minimum intensity from a stack of 250 images in which a portion of the melt-pool is visible. Comparing the traces shown in figure 4(f) with the schematic flow lines shown in figure 1 reveals a general agreement between the traces observed in this work and the flow direction suggested by Guo *et al.* [11] on the outer surface of the melt-pool. However, it is also evident from figure 4(f) that the tungsten particles entering the melt-pool on its outer surface typically only have a sufficient residence time to be conveyed to bottom of the melt-pool. This finding has important connotations for the potential use of elemental powder blends for the *in situ* creation of novel alloys as it appears to be unlikely that sufficient mixing will occur in order to achieve a homogeneous alloy composition.

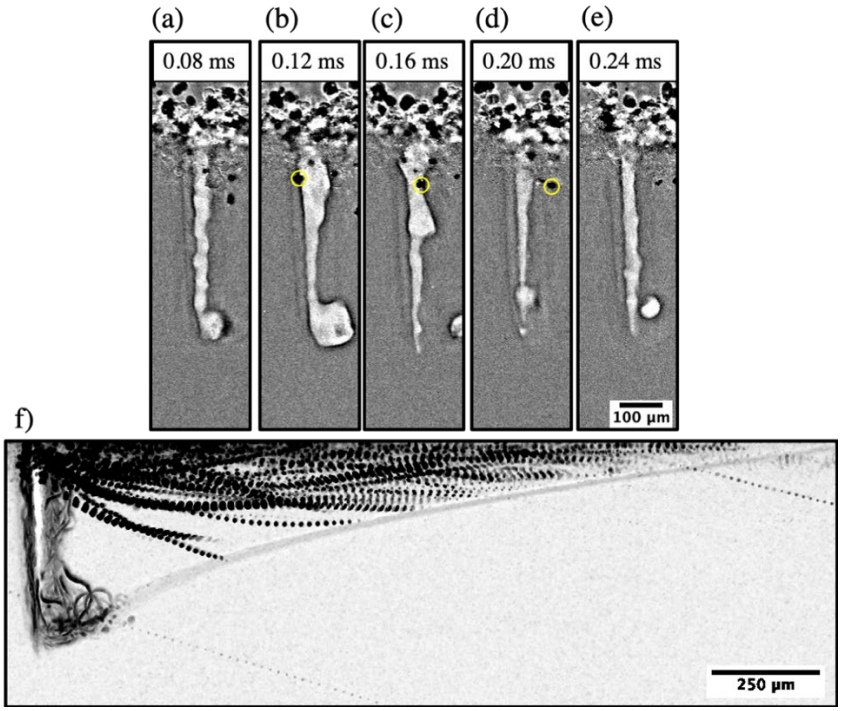

Figure 4. (a)-(e) Time series showing the progression of a tungsten tracer particle around the side of the keyhole. (f) The trajectories of tungsten tracers through the entire reconstructed melt-pool.

4. Conclusions

The nature of the melt-pool flow has been captured in the LPBF of Al-6061 using fine tungsten flow tracing particles using synchrotron x-ray radiography. It was observed in the processing parameters adopted that the flow tracing particles did not enter the melt-pool via the thin film of melt ahead of the keyhole rather they bypassed the keyhole being conveyed around its outer periphery. It is concluded that the powder particles ahead of the melt-pool in the direct path of the laser are complexly denuded via entrainment in the high-velocity vapor jet emanating from the keyhole. It is observed that the tungsten particles entering the melt-pool on its outer surface typically only have a sufficient residence time to be conveyed to bottom of the melt-pool. This highlights one of the challenges of developing processes exploiting elemental powder blends for the *in situ* creation of novel alloys. It is suggested that insufficient mixing will occur in order to achieve a homogeneous alloy composition. This experiment provides valuable data and process guidance for the optimization of LPBF and can be used to inform the development and validation of multiphysics models. Specifically, it is suggested the visualization and evaluation of the melt-pool depth, length, keyhole dimensions and melt-pool flow directions and magnitude enable the modelling community to validate complex multiphysics models.

Acknowledgements

This research is supported under MAPP: EPSRC Future Manufacturing Hub in Manufacture using Advanced Powder Processes (EP/P006566/1) and a Royal Academy of Engineering Chair in Emerging Technology. We also acknowledge the use of facilities and support provided by the Research Complex at Harwell and thank the Advanced Photon Source for providing the beam-time (213874) and staff at the 32-ID beamline for their assistance.

References

[1] Qiu C, Panwisawas C, Ward M, Basoalto H C, Brooks J W and Attallah M M 2015 *Acta Mater.* **96** 72–9
[2] Woods R A and Milner D R 1971 *Weld. J.* **50** 163–73

[3] Heiple C R and Roper J R 1982 *Weld. J.* **61** 97-102
[4] Kou S and Sun D K 1985 F *Metall. Trans. A* **16** 203–13
[5] Lee P D, North T and Perrin A R 1988 *Model. Control Cast. Weld. Process. IV* ed A F Giamei and A G J pp 131–40
[6] Lee P D, Quested P N and McLean M 1998 *Philos. T. R. Soc. A Math. Phys. Eng. Sci.* **356** 1027–43
[7] Mills K C, Keene B J, Brooks R F and Shirali A 1998 *Philos. T. R. Soc. A Math. Phys. Eng. Sci.* **356** 911–25
[8] Aucott L *et al.* 2018 *Nat. Commun.* **9** 1–7
[9] Nakamura H, Kawahito Y, Nishimoto K and Katayama S 2015 *J. Laser Appl.* **27** 032012
[10] Leung C L A, Marussi S, Atwood R C, Towrie M, Withers P J and Lee P D 2018 *Nat. Commun.* **9** 1–9
[11] Guo Q, Zhao C, Qu M, Xiong L, Hojjatzadeh S M H, Escano L I, Parab N D, Fezzaa K, Sun T and Chen L 2020 *Addit. Manuf.* **31** 100939
[12] Kang N, Coddet P, Dembinski L, Liao H and Coddet C 2017 *J. Alloys Compd.* **691** 316–22
[13] Hanemann T, Carter L N, Habschied M, Adkins N J E, Attallah M M and Heilmaier M 2019 *J. Alloys Compd.* **795** 8–18
[14] Leung C L A, Marussi S, Towrie M, del Val Garcia J, Atwood R C, Bodey A J, Jones J R, Withers P J and Lee P D 2018 *Addit. Manuf.* **24** 647–57
[15] Leung C L A, Marussi S, Towrie M, Atwood R C, Withers P J and Lee P D 2019 *Acta Mater.* **166** 294–305
[16] Zhao C, Fezzaa K, Cunningham R W, Wen H, De Carlo F, Chen L, Rollett A D and Sun T 2017 *Sci. Rep.* **7** 1–11
[17] Guo Q, Zhao C, Escano L I, Young Z, Xiong L, Fezzaa K, Everhart W, Brown B, Sun T and Chen L 2018 T *Acta Mater.* **151** 169–80
[18] Zhao C, Guo Q, Li X, Parab N, Fezzaa K, Tan W, Chen L and Sun T 2019 *Phys. Rev. X* **9** 021052
[19] Matthews M J, Guss G, Khairallah S A, Rubenchik A M, Depond P J and King W E 2016 *Acta Mater.* **114** 33–42
[20] Matthews M J, Guss G, Khairallah S A, Rubenchik A M, Depond P J and King W E 2017 *Addit. Manuf. Handb. Prod. Dev. Def. Ind.* **114** 677–93
[21] Bidare P, Bitharas I, Ward R M, Attallah M M and Moore A J 2018 *Acta Mater.* **142** 107–20